

# Precision Photometry for Q0957+561 Images A and B

Wesley N. Colley and Rudolph E. Schild

Harvard-Smithsonian Center for Astrophysics, 60 Garden Street, Cambridge MA 02138

## ABSTRACT

Since the persuasive determination of the time-delay in Q0957+561, much interest has centered around shifting and subtracting the A and B light-curves to look for residuals due to microlensing. Solar mass objects in the lens galaxy produce variations on timescales of decades, with amplitudes of a few tenths of a magnitude, but MACHO's (with masses of order  $10^{-3}$  to  $10^{-7}M_{\odot}$ ) produce variations at only the 5% level. To detect such small variations, highly precise photometry is required.

To that end, we have used 200 observations over three nights to examine the effects of seeing on the light-curves. We have determined that seeing itself can be responsible for correlated 5% variations in the light-curves of A and B. We have found, however, that these effects can be accurately removed, by subtracting the light from the lens galaxy, and by correcting for cross contamination of light between the closely juxtaposed A and B images. We find that these corrections improve the variations due to seeing from 5% to a level only marginally detectable over photon shot noise (0.5%).

*Subject headings:* techniques: photometric — methods: data analysis — quasars: individual (0957+561) — gravitational lensing — galaxies: halo — dark matter

## 1. Introduction

The attempts to observe quasar brightness fluctuations to measure time delays and detect microlensing have shown that a high level of photometric accuracy is desirable. For Q0957+561 (Walsh et al. 1979) a substantial controversy about the time delay persisted for more than a decade despite reliable photometry on 1000 nights (Kundić et al. 1997, Schild 1990, Vanderriest et al. 1989, Press et al. 1992b, Haarsma et al. 1996). Part of the confusion could have been due to microlensing, which is difficult to distinguish from intrinsic quasar fluctuations, upon which the time delay measurements are leveraged. The observational evidence suggests that microlensing has a component due to solar mass stars

causing fluctuations on time scales of decades and amplitudes of a few tenths of a magnitude (Schild & Smith 1991, Pelt et al. 1998). However, it is possible that there exists a more rapid microlensing component due to MACHO’s in the lens galaxy’s halo (Schild 1996, Young 1981, Gott 1981). Such fluctuations occur at the few percent level; thus photometry of both images is required to have a precision of 0.01 magnitudes or better.

A very large data base for the Q0957 system has been collected from CCD data frames since 1979 and reduced on several generations of computers, but the basic photometric procedure has been the same. Aperture photometry with 6" diameter apertures, and correction for an  $R \approx 18.3$  lens galaxy in the B aperture, have been the basis throughout, and many procedural details and error considerations have been given in the appendix of Schild and Cholfin 1986. The most problematic aspect of the reduction scheme is the bleeding of light from one quasar image to the aperture of the other, particularly when seeing is poor due to turbulence in the terrestrial atmosphere. In principle it should be possible to estimate and correct for the effect by examining the spread of light from nearby field stars, but attempts to implement correction schemes have failed in the past, probably because they have not taken into account the light of the lens galaxy G1, which has an extended profile and is situated between the two quasar images. Thus it has been recognized that significant improvement in the photometric precision would be achieved only when an image from the Hubble Space Telescope could be analyzed to measure the brightness profile of lens galaxy G1.

Bernstein et al. (1997) have recently used the HST to image the lens system, so that it is now possible to make accurate estimates of the contribution of light from lens galaxy G1 to the A and B apertures, and thence, to correct for the spillover of light from one quasar image into the aperture of the other. The purpose of this contribution is to establish the method of improved aperture photometry, and to demonstrate its use on a data set consisting of 200 images collected on three nights in February, 1995, when both quasar images were not showing large brightness fluctuations. Of course the most trustworthy observation of quasar variability is one which shows no variability, and the available data allow us to effectively compare our measurement uncertainty limits with Poisson statistics.

## 2. Photometry Scheme

For over a decade, RS has monitored Q0957 and amassed a “master dataset” of the variations of images A and B (Schild & Thompson 1995). Our 1k×1k CCD images have pixel scales of one-third of an arcsecond, exposure times of 450 seconds, read-noise of  $8e^-$ , and FWHM seeing of 1.5–2 arcseconds. This generally allows for about 5 unsaturated,

well sampled comparison stars in the  $R$ -band on each data-frame. There are thousands of such frames, and together, they represent one of the largest continual monitoring efforts in history.

Since the amount of archived data is large, an automated photometry code (one that does not require mouse clicks, or manual entry of parameters) is desirable. Interfacing all of the necessary photometry, pre-processing and post-processing code proved to be easiest for WNC in the IDL programming language, at cost of some redundancy with available photometry packages in IRAF.

The photometry algorithms we have used are modelled after those in IRAF, *daofind*, for example. First the flat-fielded image is convolved with a “lowered Gaussian” kernel with width similar to that of the seeing. The lowered Gaussian is a two-dimensional Gaussian bell, less a constant. The constant equals the volume under the Gaussian, out to two-sigma, where the convolution kernel terminates. A threshold is selected in terms of the standard deviation of noise in the sky, and pixels above that threshold are tabulated. We then use a friend-of-friend algorithm to group adjacent high pixels from the list. These groups are presumed to reside at the locations of sources. Typically, this algorithm locates about 15–20 sources per frame.

In order to understand which source is which, we first generate a template list of sources, which contains only the 10 sources we are interested in, two of which are the QSO images A and B. This list contains only the relative astrometry for each source (in pixels). For each data frame, we generate aperture astrometry for each of the sources located by the friend-of-friend algorithm above. We then compute the pixel position angles of each source relative to a particular source in the template and data source list. The correlation function of the data angles with the template angles reveals a peak at the correct angular offset between data sources and template sources. One can iterate for a few sources, and determine the magnification, rotation and translation of the data source list relative to the template source list, from which the positions of all the template stars on the data frame are determined. This scheme is particularly useful, because without clever thresholding the quasar images tend to blend together, or disappear completely. But after the geometry of the field is determined, one can compute the locations of the quasar images with little difficulty.

The final complication is cosmic rays. Since we would like to use each exposure, we do not have the luxury of medianing several exposures to remove cosmic rays. Furthermore, we would like to avoid visual inspection as the cosmic ray detector. Our automated cosmic ray detection scheme generates a model point spread function by co-adding several of the sources on each frame (we will need this model p.s.f. for the galaxy subtraction anyway).

We then fit this model to each of the sources. A large spike in the post-fit residual from any source is interpreted as a cosmic ray, and the source is thrown out of the reduction. Only occasionally (a few times per night) is a source lost from the reduction.

With the useful source positions now determined hands-free, the aperture photometry is straight-forward. First, sky values are obtained as the median flux in an annulus around each source, 30 to 60 pixels in radius; then, the fluxes within circular apertures, less sky, are tabulated.

At risk of being pedantic, we have plotted in Figure 1 the raw light-curve for the “A” (northern) image of Q0957+561 at top. The errorbars reflect Poisson uncertainty. Because of weather and seeing, this raw aperture photometry varies by more than 1.5 magnitudes, for an object that should have approximately constant brightness over three nights. With respect to the mean, this light-curve yields a reduced  $\chi^2$  of 1300 per degree of freedom. Obviously, this is why one uses relative photometry (versus absolute photometry), and at bottom, we have plotted the photometry of the A image relative to that of comparison stars in the field, using the Honeycutt (1992) method for ensemble photometry, and as expected the improvement is vast ( $\chi^2 \sim 9$  per d.o.f.).

The Honeycutt (1992) method proves to be quite effective at producing a good estimate of the relative brightness of objects on the same frame (c.f. Kundić et al. [1995 and 1997]), and this is the typical level of sophistication with which light-curves of 0957+561 have been produced (ibid). Such light-curves, however, often contain nagging correlations between the “A” and “B” images night to night. After some effort to understand these correlations as possible effects of moon phase, or other astronomical situations, the A-B correlations remain largely unexplained.

Returning to Figure 1, we can see that even after the Honeycutt correction, there remains a 5% departure from the mean magnitude on the third night. This is particularly troubling for an object which is generally not supposed to vary by more than about 0.01 magnitudes per day (Press et al. 1992b; Keel 1982); hence, the 5% variation over several hours must be due to some observational condition. We will show that this departure is due principally to seeing, and its daughter effects, namely changing characteristics of light from the galaxy, and cross contamination of light between the two quasar images (separated by 6”) during poor seeing.

### 3. Galaxy Subtraction

One effect of seeing arises because the giant elliptical lens galaxy, “G1,” has a rather cuspy profile. This profile gets smeared over larger and larger radii as seeing deteriorates. Since the core of G1 is only 1" from the B image, most of the galaxy’s light lies within the image B aperture, but outside the A aperture. One would therefore expect poor seeing to introduce more galaxy light into the image A aperture, and remove some light from the image B aperture. Since the galaxy has a an  $R$  magnitude of 18.3 (about 15% of the image B brightness), changes of order 10% in the galaxy’s contribution can introduce effects of order 1–2% in the measured flux from images A and B, a level that we are very much interested in.

Additionally, since 15% is quite significant (the fraction would be smaller at shorter wavelengths), removal of the galaxy is critical to proper treatment of the cross-talk problem, which we will discuss in the next section—there we will need to know the relative amounts of light in each aperture from the quasar itself, before the apertures were polluted by the galaxy.

To correct for the galaxy contamination, we have taken advantage of published HST imaging of galaxy G1 (Bernstein et al. 1997). Those authors computed best-fit elliptical isophotes for the galaxy, and we have used their plots of ellipticity, position angle and surface magnitude (as functions of semi-major axis, their Fig. 2.) to produce synthetic galaxy images for each data frame.

To determine the appropriate zero-point for the galaxy, we use the relative magnitude shown in Bernstein et al. (1997) Fig. 2 between Kitt Peak  $R$ -band data and  $HST$   $F555W$  data for the galaxy’s brightness profile. We find that the correction,  $F555W - R = 1.2$ , is very close to the correction expected for an elliptical galaxy at  $z = 0.36$  (Fukugita, Shimasaku & Ichikawa 1995). Note that no allowance for a color gradient has been made. Ideally,  $HST$  imaging in redder bands, such as  $F606W$  and  $F850W$ , would exist, so that minimal color corrections would be necessary.

In order to synthesize the galaxy, we start with an image 4 times oversampled in both dimensions, and compute the semi-major axis at each pixel, while carefully observing dependences of ellipticity, and position angle on semi-major axis (Bernstein et al. 1997). The pixels within this image are then sampled dynamically, according to semi-major axis. Those pixels closest to the center are oversampled an additional  $32 \times 32$  times, and those farther out are sampled exponentially less frequently such that the farthest pixels are sampled once. In each subpixel is placed the correct flux, according to the surface brightness dependence on semi-major axis (Bernstein et al. 1997). The dramatic oversampling ensures

that the steeply increasing flux near the center is well-sampled, and we find that this process results in flux error of a few parts per 1000 in any given pixel (on the large  $4 \times 4$  oversampled image).

We then rotate and demagnify the  $4 \times 4$  oversampled image, so that it appears at the correct pixel scale and position angle according to astrometry from the the data image. The rotation and demagnification involves cubic spline interpolation within the *ROT* routine provided by IDL. We convolve this properly sized and oriented image with the point spread function, which we have previously obtained from comparison stars on the data frame.

To determine the proper zero-point for the galaxy, one must be aware that simple aperture photometry from the comparison stars may not suffice. When seeing degrades, a non-negligible fraction of the light from a given star can seep out of the aperture. While the effect is similar for all point-sources on the frame, the relative change in brightness differs significantly for resolved objects, such as galaxy G1. One should therefore calibrate a resolved object with the “total” light from the comparison point-sources. To assess the “total” light, we used a series of apertures of different size as input into an implementation of *Numerical Recipes’ ratint.f* rational function extrapolator (Press et al. 1992a). We could then extrapolate to a very large aperture to estimate the total light. However, in practice, we found that even in the worst seeing conditions an aperture of diameter 20 arcseconds contained all the light to the 1–2% level, and avoided the larger errors introduced by extrapolation. We therefore calibrated the synthesized galaxy flux with this very large aperture photometry from several comparison stars on the field.

We now have a properly located, scaled and oriented convolved image to subtract from the data frame, and after doing so, we perform the aperture photometry on the A and B images once again. In Figure 2, we have plotted a contour map of the quasar images from a typical exposure, before and after the galaxy subtraction. The solid contours correspond to flux on the data frame after galaxy subtraction, the dashed contours to flux before galaxy subtraction. We include, for reference, contours of the synthesized galaxy, with much fainter contour levels, of course. Notice the improvement in similarity between the shapes of the image A and B contours: before galaxy subtraction, the B image had significant extension in the northward direction, due to the excess light from the galaxy. The subtraction removes that extension effectively.

In Figure 3, we have plotted, as a function of seeing, the fraction of total light in the A and B apertures due to the galaxy. As suspected, the image B photometry declines with poor seeing because more light from the core of the galaxy is getting smeared out of the aperture. The A image, however, is far from the center of the galaxy, so that the smearing of bright parts of the galaxy out to larger and larger radii increases the light from the

galaxy in the A image, which is visible in Figure 3. These two effects conspire to produce a relative change of up to 2.5% from good to bad seeing, which, in itself, should be corrected.

#### 4. Cross Talk Correction

Another effect of seeing is “cross talk” between the images A and B, particularly during bad seeing. Since the images are separated by only 6”, apertures of 6” (diameter) practically rub against each other, so light spilled out of one aperture due to seeing can very easily wind up in the other aperture.

We have attempted to address this concern in a simple way. After proper galaxy (and sky) subtraction, the aperture fluxes of images A and B should represent only light from the quasar. If that’s true, the comparison stars in the frame should exhibit the same fraction of spillover of light into nearby apertures as do the quasar images.

We selected apertures about nearby comparison stars; these apertures were offset from the comparison stars at the same pixel offset as that between images A and B (see Figure 4 test apertures AB and BA). The amount of light in these fiducial apertures as a fraction of the recorded aperture flux from the comparison star should be identical to the fraction of cross talk light from each quasar image. We define  $r_{BA}$  as the ratio of the light in test aperture BA to the aperture flux of the comparison star, with similar definition for  $r_{AB}$ . Note that  $r_{BA}$  estimates the ratio of the spilled light from image B into the A aperture, to the actual light from image A in the A aperture.

To correct for cross talk, we compute the corrected fluxes of A and B as

$$\begin{aligned} A_{corr} &= (A_{meas} - r_{BA}B_{meas}) \cdot (1 - r_{AB}r_{BA})^{-1} \\ B_{corr} &= (B_{meas} - r_{AB}A_{meas}) \cdot (1 - r_{AB}r_{BA})^{-1} \end{aligned} \tag{1}$$

where  $A_{meas}$  is the measured flux,  $A_{corr}$  is the corrected flux,  $r_{BA}$  is described above, and the complementary variables transposing A with B obey the same notation. The denominator compensates for the overcorrection made while subtracting  $r_{BA}B_{meas}$  when  $B_{meas}$  is contaminated by light from A.

We plot in Figure 5 the  $r_{AB}$  (triangles) and  $r_{BA}$  (circles) as a function of FWHM seeing. As expected, with good seeing, the fraction is quite small, but with poor seeing, the fraction can approach 5%, which is a substantial correction for our purposes.

## 5. Final Light-curves

In Figures 6 a, b and c, we have plotted the light-curves from the nights February 6–8, 1995. In each case we have used the Honeycutt (1992) method for ensemble photometry to correct for the “exposure magnitude” as was done in Figure 1.

Figure 6a shows the raw aperture magnitudes of the A and B images. On the third night, particularly, there is an obvious hump in the light-curve of both A and B, on the order of a few percent, but notably greater in A than in B.

Figure 6b illustrates how the galaxy subtraction effects the light-curves. First of all, image B is dimmed by about 15%, consistent with Figure 3. The hump on the third night remains, but notice that it has become more equal in amplitude in images A and B. The hump itself has occurred mainly because of the cross talk problem as the seeing degraded substantially. However, we can understand how the galaxy’s light affects the amplitude of the hump if we recall Figure 3. Figure 3 demonstrated that as the seeing degraded, the galaxy contributed more light to the A aperture, but less light to the B aperture. Hence the seeing induced hump is more pronounced in A than in B. Our galaxy subtraction has allowed for this difference, and the amplitude of the hump has come more into agreement between the two images.

Figure 6c contains the final light-curves after correcting for the cross talk problem. Notice the removal of the hump on the third night.

The improvement in the light-curves after the two corrections can be quantified, but we must first compute the errorbars. In Figure 6a, with no corrections, the errors are simply Poisson noise:  $\Delta\text{flux}$  (in counts) =  $[\text{flux} + \text{sky}]^{1/2}$ . In Figure 6b, the total flux of the comparison stars for the galaxy has been calculated, and added fractionally to the errorbar:

$$\sigma_{A_{gal}}^2 = A_{gal}^2 \cdot \left[ \sum_{i=1}^{N_*} \text{flux}_i \right]^{-1}, \quad (2)$$

where  $A_{gal}$  is the flux in the A aperture from the galaxy, and the sum is the total light from the comparison stars, which serve as the zeropoint for the galaxy model. This  $\sigma_{A_{gal}}$  is, of course, added in quadrature to the Poisson errorbars in Figure 6a. Figures 6c and d require an additional error term, from the comparison stars in the cross talk calculation. This term is rather more complicated, because a derivative of equation 1 is required, so for sake of brevity, we will omit the derivation. Suffice it to say that the errorbar variances have the familiar additional first order term,

$$\sigma^2(g) = \left( \frac{\partial g}{\partial f} \right)^2 \sigma^2(f). \quad (3)$$



In Table 1, we have listed the mean errorbar for each method. As expected they increase slightly with the introduction of the corrections. We have also included the (reduced)  $\chi^2$  deviation from zeroth, first and second order polynomial fits to the data, which can be seen in Figure 7 (one would not expect variations much more complicated than second order, because the maximum change in one day is of order 1% [Press et al. 1992b]). In each case the  $\chi^2$  improves by at least 50%, and as much as 700% from the raw data to the corrected data, with little penalty in the mean error-bar of each point. The corrected photometry is typically reliable to about 0.55% (5.5 millimagnitudes), within about 10% ( $\chi^2 \sim 1.2$ ) of Poisson error. This can be compared with the roughly 5% (50 millimagnitudes) reliability of the uncorrected A image (see Figure 6a).

As a final comment, we note that Figure 6 illustrates how a zero time-delay correlation could appear in work such as Kundić et al. (1995 and 1997). The uncorrected light-curves of images A and B (Figure 6a) appear very much correlated, as we can see in the last two columns of Table 1, where we have listed the estimated Pearson correlation coefficient ( $\rho_{AB} = \sigma_{AB} \cdot [\sigma_A \sigma_B]^{-1}$ ) for the data relative to the mean, and relative to the best-fit parabolas ( $\rho_{AB,0}$  and  $\rho_{AB,2}$ , respectively). Without getting into an involved statistical discussion, we note that the value of  $\rho_{AB}$  improves dramatically after correction for cross talk. The value of  $\rho_{AB} = 0.76$  has a chance of less than 1 in  $10^{36}$  to arise from uncorrelated Gaussian deviates, while a value of  $\rho_{AB} = 0.22$  would arise 2.1 times out of a thousand (Lupton, 1993). After subtraction of the best-fit parabolas for the three cases, the correlation coefficients  $\rho_{AB,2}$  decrease in each case, and while the value of 0.59 is only likely at the 1 in  $10^{19}$  level, the value of 0.13 is 7% likely to arise from uncorrelated Gaussian variates. While the exact meaning of these statistical probabilities is debatable, the corrections obviously dramatically reduce statistical correlations in the photometry. These improvements make it easy to see that seeing could explain some of the zero-delay correlations in Kundić et al. (1995 and 1997) and in other monitoring projects as well.

Note, however, that the constancy of the quasar brightness found here is comparable to that of photometry reported in Schild & Thompson (1996). This is not surprising because the Schild photometry results from some censoring of data during bad seeing (to avoid the problems detailed here). Thus, for example, data for Nov. 1998, show a total r.m.s. deviation of only 0.013 magnitudes, as reported in Schild (1990).

## 6. Summary and Conclusions

In order to search for microlensing in Q0957+561, it will be necessary to process large number of data frames taken over more than a decade. A highly automated program

for photometry is desirable. We have therefore created a hands-free system of generating reliable photometry for this object.

Furthermore, we have introduced methods to treat the problems related to changing seeing that have plagued photometry of this object in the past. One problem is that seeing changes the amount of light introduced by the lens galaxy into apertures about the A and B images. A second problem is that bad seeing causes cross contamination of light from one image into the other. These effects conspire to cause correlated errors of up to 5% in the photometry. This is at approximately the same level as variations expected from microlensing by small stars and MACHO's in the lens galaxy, and is thus necessary to remove.

We have greatly improved the situation by 1) using HST data to subtract the lens galaxy, 2) using comparison stars to estimate the level of cross talk between the images. After these corrections, we find that the photometry is reliable to about 5.5 millimagnitudes (0.55%) for a single image frame, a vast improvement over 5% in the uncorrected photometry. The fact that the corrections for seeing practically eliminate correlated errors suggests that the seeing is the principal cause for these errors.

With these methods to correct for seeing, we plan to reduce large amounts of archival data on Q0957+561 and search for microlensing by discrete objects within the lens galaxy. To date, a handful of events at the 5% level are suggested by observation (Schild 1996), which Schmidt & Wambsganss (1998) have used to put important limits on allowed masses for MACHO's (assuming small QSO source size). With much improved photometry on the many more observations available to us, we will be able to characterize with some confidence the masses and densities of MACHO's in the Q0957 lens galaxy.

## REFERENCES

- Bernstein, G., Fischer, P., Tyson, J. A., & Rhee, G., 1997, *ApJ*483, L79
- Fukugita, M., Shimasaku, K., & Ichikawa, T. 1995, *PASP*, 107,945
- Gott, J. R. 1981, *ApJ*, 243, 140
- Haarsma, D. B., Hewitt, J. N., Lehár, J., & Burke, B. F. 1996, *ApJ*, submitted (astro-ph/9607080)
- Honeycutt, R. K. 1992, *PASP*, 104, 435
- Keel, W. C. 1982, *ApJ*, 255, 20
- Kundić, T., Colley, W. N., Gott, J. R. III, Malhotra, S., Pen, U., Rhoads, J. E., Stanek, K. Z., & Turner, E. L. 1995, *ApJ*, 455, L5
- Kundić, T., Turner, E. L., Colley, W. N., et al. 1997, *ApJ*, 482, 75
- Lupton, R. H. 1993, *Statistics in Theory and Practice* (Princeton: Princeton Univ. Press), §12.3
- Pelt, J., Hjorth, J., Refsdal, S., Schild, r., & Stabell, R. 1998, *A&A*, in press
- Press, W. H., Flannery, B. P., Teukolsky, A. S., & Vetterling, W. T. 1992a, *Numerical Recipes* (Cambridge: Cambridge Univ. Press), p. 106
- Press, W. H., Rybicki, G. B., & Hewitt, J. N. 1992b, *ApJ*, 385, 404
- Schild, R. E. 1990, *AJ*, 100, 1771
- Schild, R. E. 1996, *ApJ*, 464, 125
- Schild, R. E., & Cholfin, B. 1986, *ApJ*, 300, 209
- Schild, R. E., & Smith, R.C., 1991, *AJ*, 101, 813
- Schild, R. E., & Thomson, D. J. 1995, *AJ*, 109, 1970
- Schmidt, R., & Wambsganss, J. 1998, astro-ph/9804130
- Vanderriest, C., Schneider, J., Herpe, G., Chevreton, M., Moles, M., & Wlérick, G. 1989, *A&A*, 215, 1
- Walsh, D., Carswell, R. F. & Weymann, R. J. 1979, *Nature*, 279, 381
- Young, P. 1981, *ApJ*, 244, 756

**TABLE 1**

method	A				B				$\rho_{AB,0}$	$\rho_{AB,2}$
	$\bar{\sigma}$	$\chi_0^2$	$\chi_1^2$	$\chi_2^2$	$\bar{\sigma}$	$\chi_0^2$	$\chi_1^2$	$\chi_2^2$		
no correction	0.0047	9.41	4.76	4.38	0.0042	3.61	2.02	2.07	0.79	0.66
galaxy subtracted	0.0048	5.45	3.02	2.86	0.0046	4.27	2.15	2.19	0.76	0.59
cross talk corrected	0.0049	1.23	1.23	1.19	0.0047	1.27	1.20	1.02	0.22	0.13

Table 1: Mean errorbars ( $\bar{\sigma}$ , in magnitudes), computed from Poisson statistics alone; and reduced  $\chi^2$  of fits to the mean magnitude ( $\chi_0^2$ ), a line ( $\chi_1^2$ ), and a parabola ( $\chi_2^2$ ), over three nights (see Figure 7). The last two column columns are the Pearson correlation coefficients of A with B, relative to their means ( $\rho_{AB,0}$ ) and to their best-fit parabolas ( $\rho_{AB,2}$ ). The first row is before any correction for the galaxy or cross talk. The second row is tabulated after the galaxy has been subtracted. The third row follows correction for cross talk.

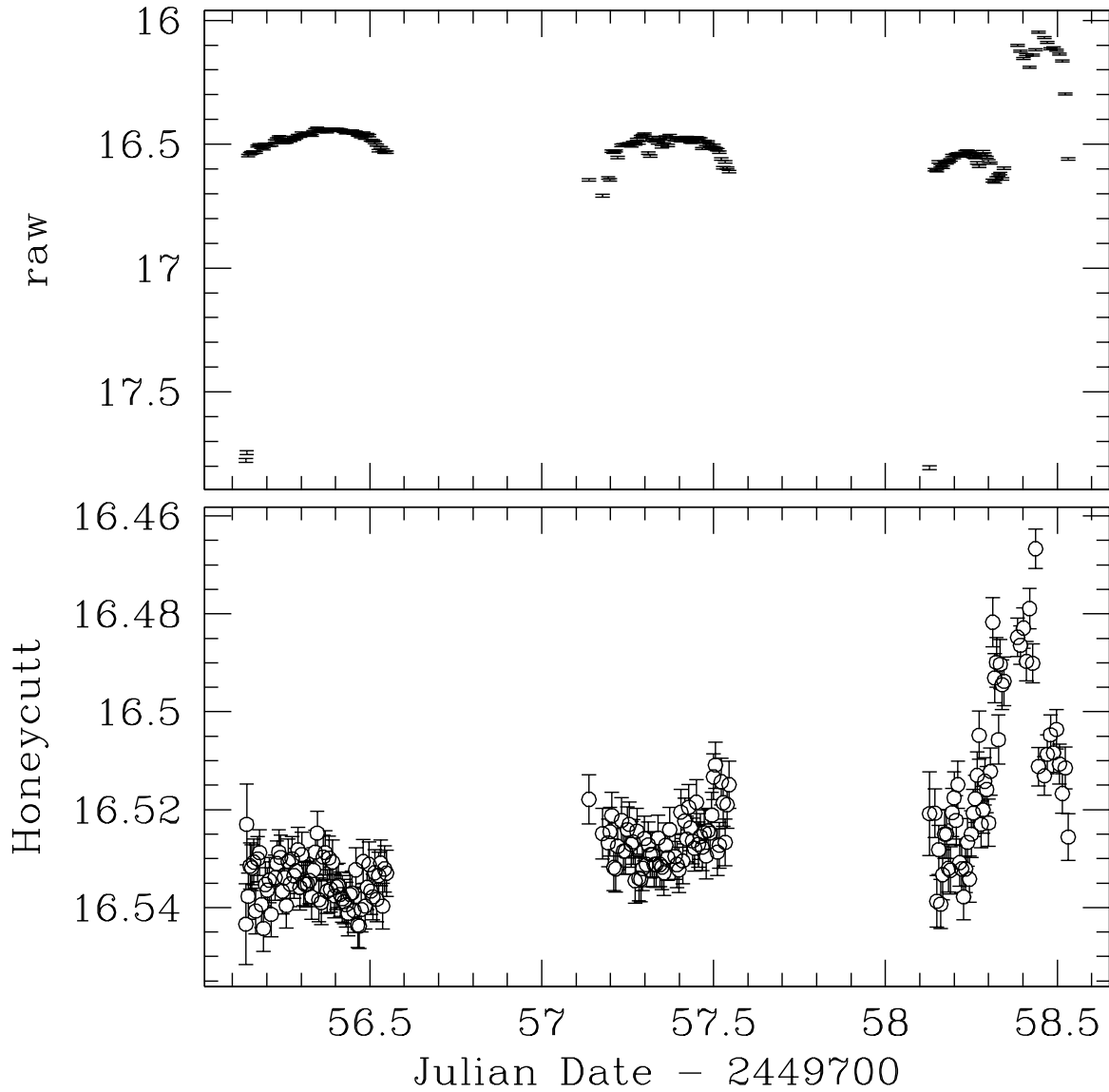


Fig. 1.— Light-curve of “A” image of QSO 0957+561, before any correction (top), and after the Honeycutt (1992) method for ensemble photometry is applied (bottom). Points have been omitted at top to allow the visibility of the expected Poisson errorbars. Errorbars at bottom also reflect Poisson noise uncertainty.

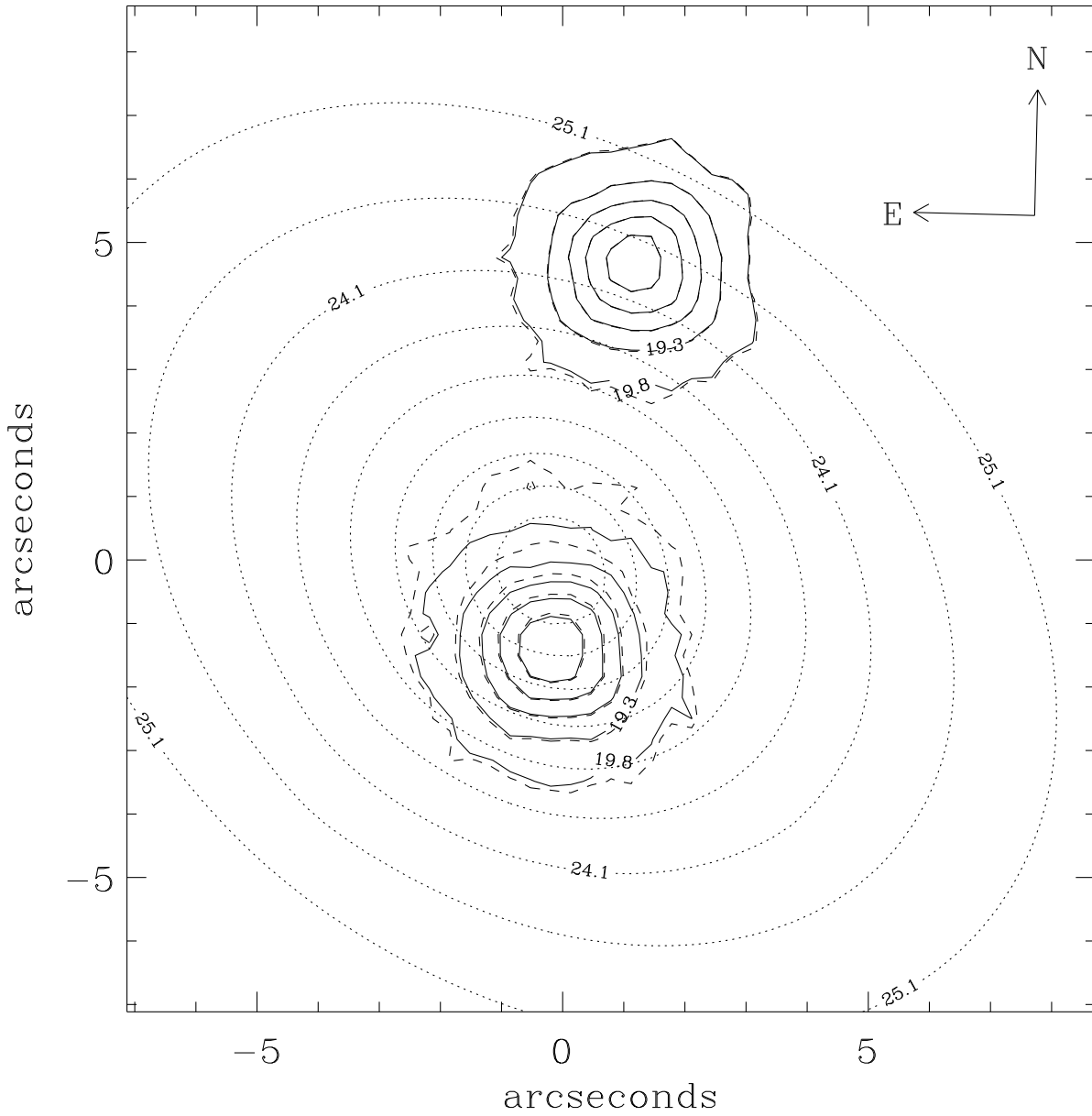


Fig. 2.— Subtraction of the lens galaxy, G1, from images of the 0957+561 system. The dotted contours are those of the galaxy image which is subtracted from the data image. The dashed contours represent the raw data image before galaxy subtraction, with image A at top, and image B in bottom center. The solid contours are after galaxy subtraction. Note the improved agreement in shape of the quasar images after subtraction of the galaxy. Please be aware that the galaxy contour levels are much fainter than those of the quasar images.

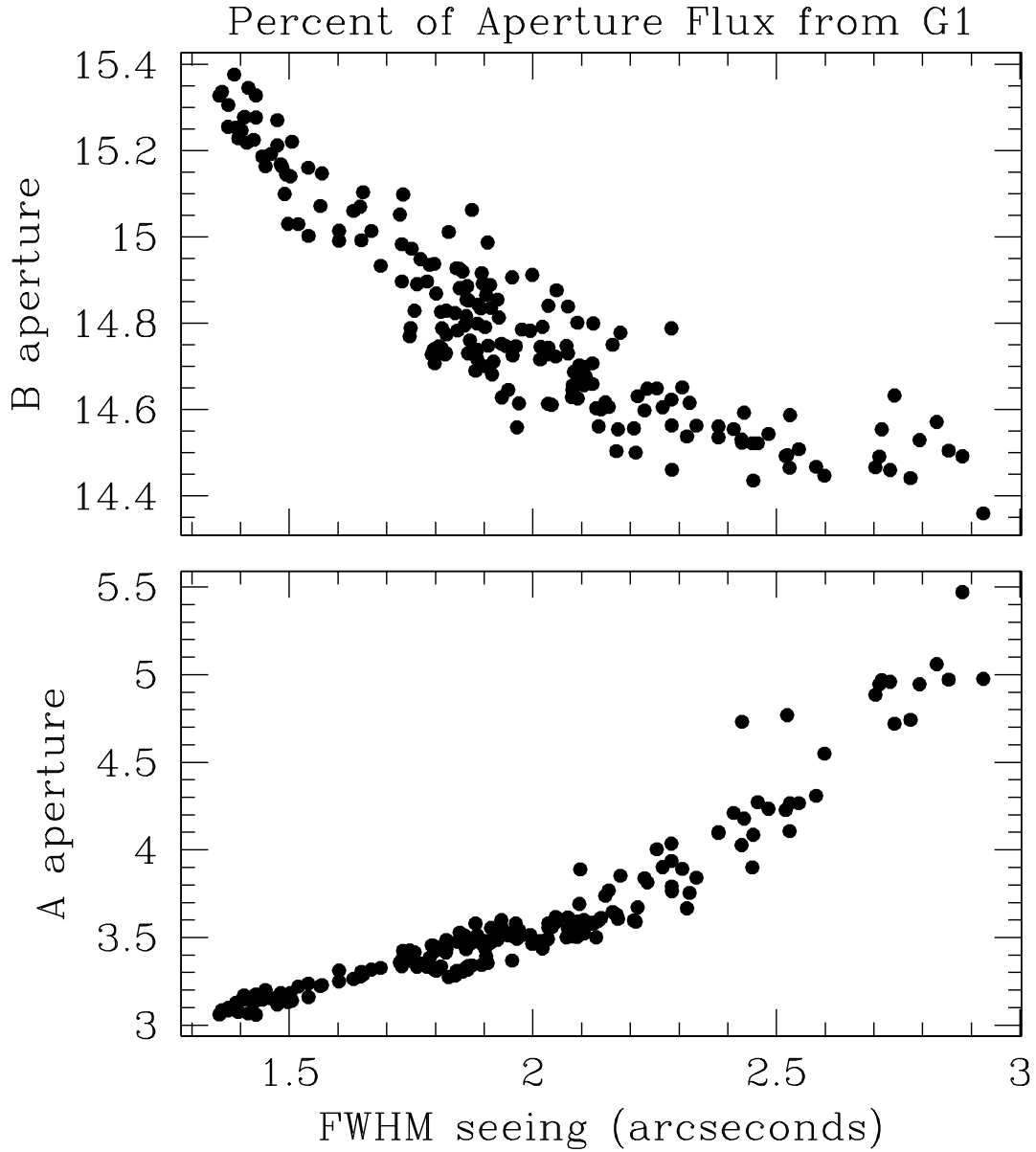


Fig. 3.— The percentage contribution of light from the galaxy G1 to the apertures about images A and B, as a function of seeing. As seeing worsens the galaxy’s core is spread more thinly out of the B aperture, causing image B apparently to dim, but image A brightens as seeing worsens, because more light from the center of the galaxy is spread into its aperture.

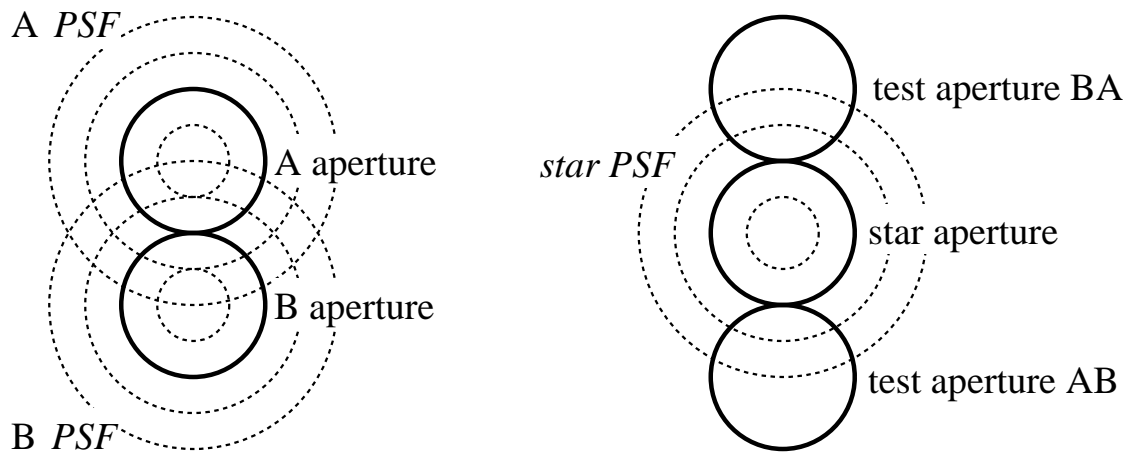


Fig. 4.— The problem of cross talk. At left, light from image A contaminates the image B aperture, and vice versa, particularly in bad seeing. At right, the solution: test apertures are drawn near a comparison star at the same pixel offsets exhibited by the A and B apertures. The contamination of the test apertures should be fractionally similar to the cross contamination of the A and B apertures.



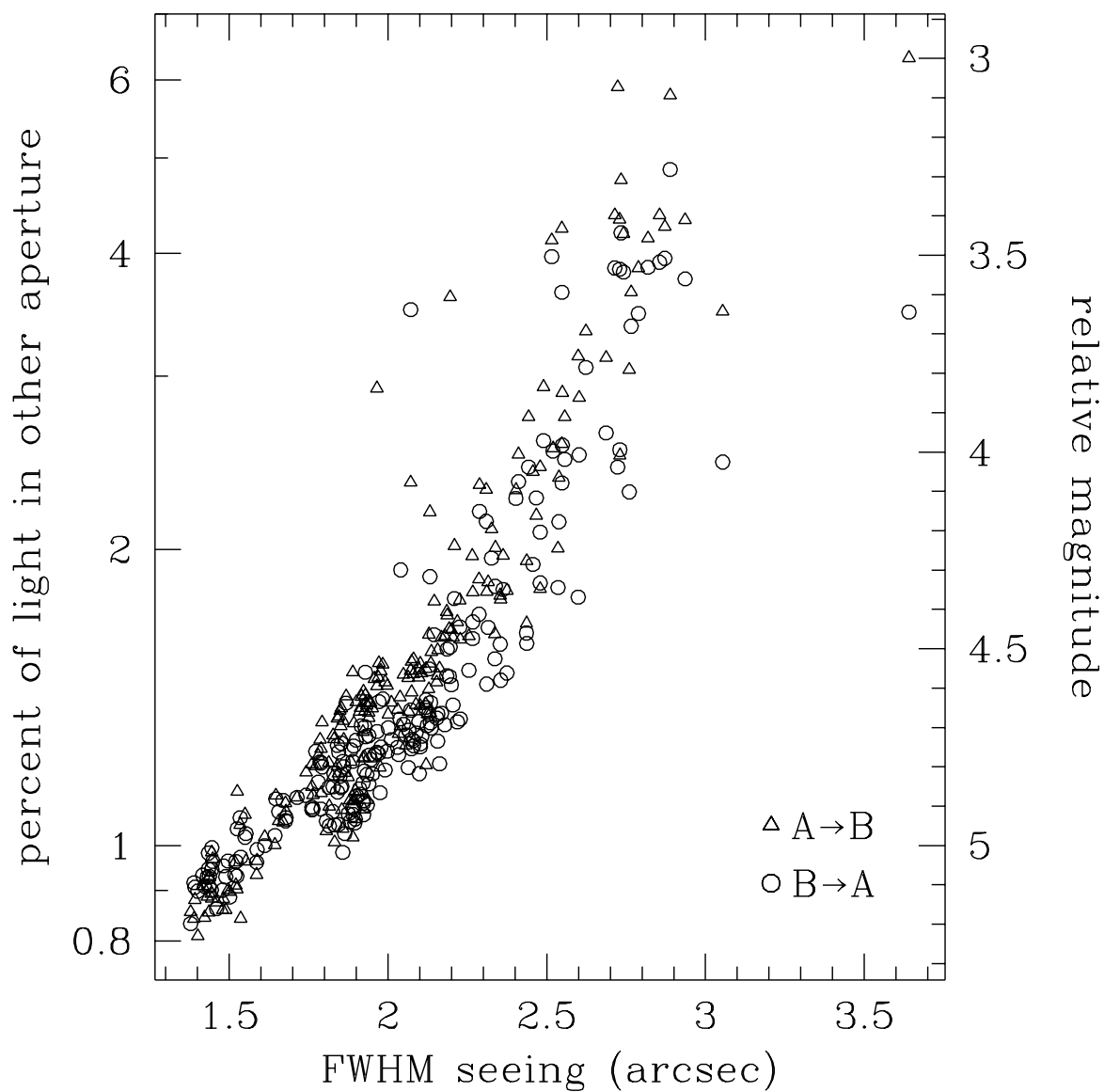


Fig. 5.— Cross talk as a function of seeing. The light from image A that spills into aperture B (see Figure 4), divided by the measured aperture flux of image A, is plotted as triangles. The corresponding interchange of A and B is plotted as circles. Notice that the ratios can approach 5%.

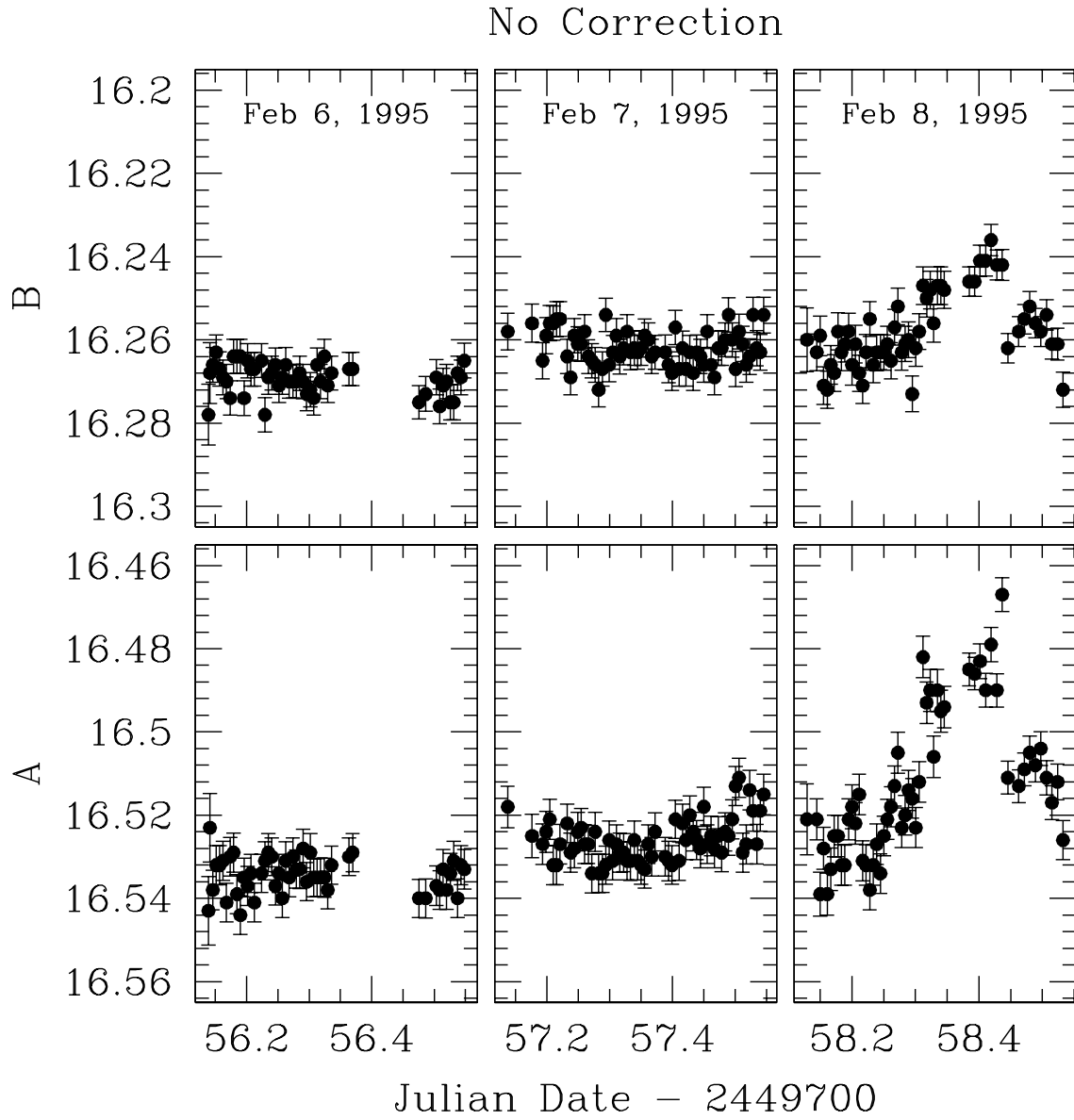


Fig. 6.— a) The light-curve of images A and B after use of the Honeycutt (1992) method for ensemble photometry. Notice the large (few percent) hump on the third night, which occurs in both the A and B images.

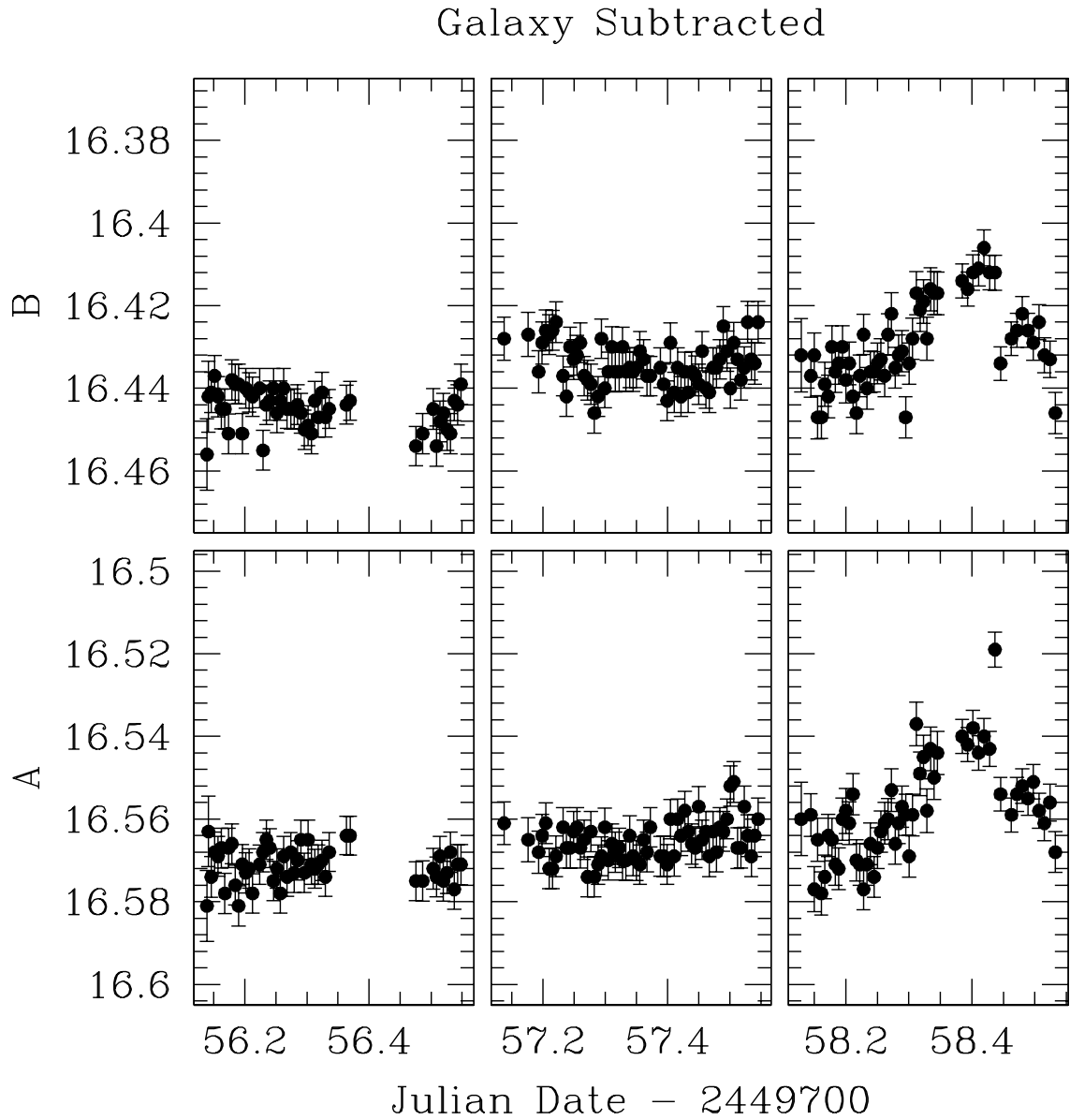


Fig. 6.— b) The light-curve of images A and B after subtraction of the galaxy G1's contribution to the A and B apertures. The large hump in the A light-curve has been reduced to a level similar to that of the B light-curve.

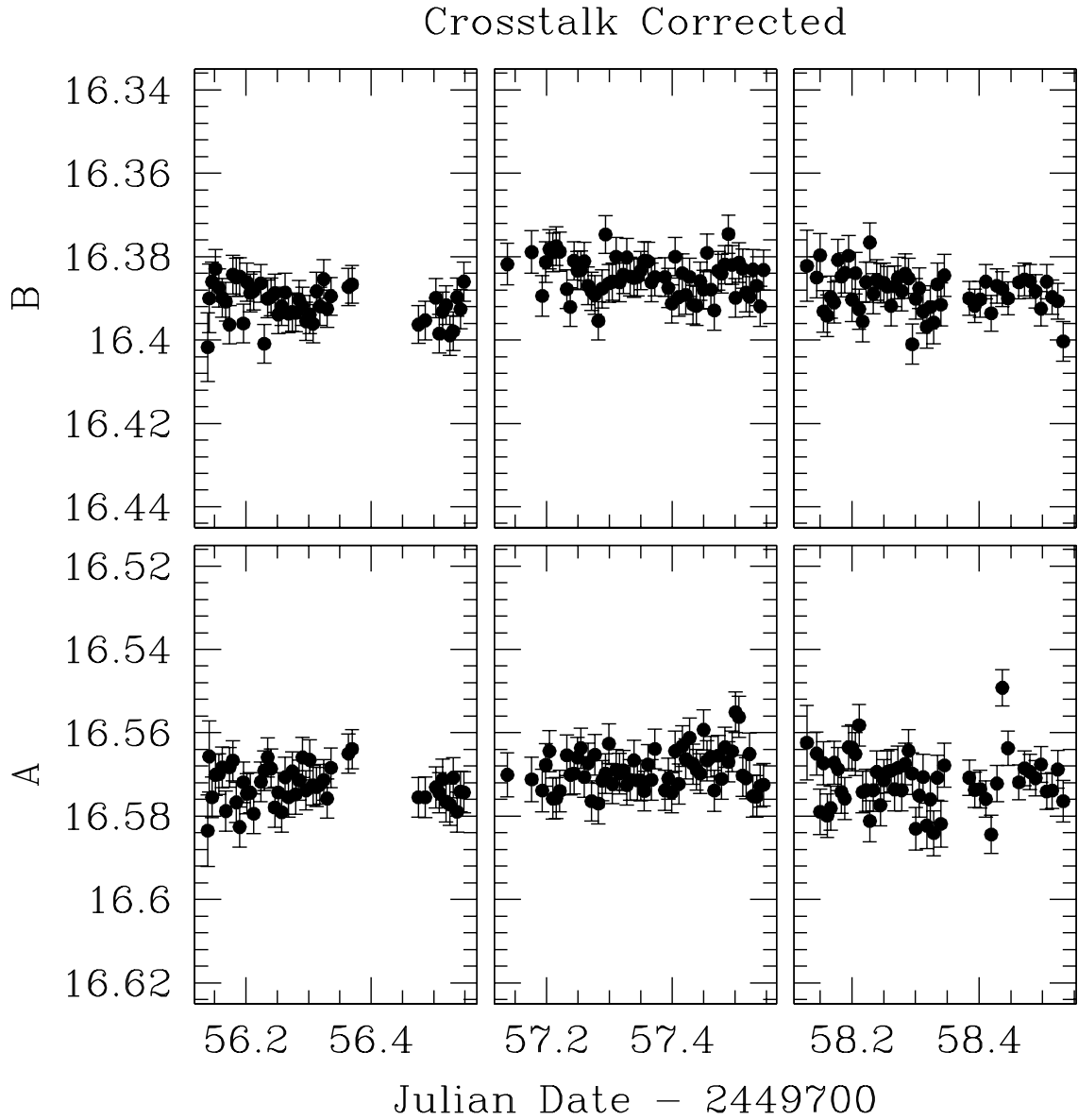


Fig. 6.— c) The light-curve of images A and B after subtraction of the galaxy G1 and correction for “cross talk.” Cross talk is the spill-over light from the quasar images A and B into each other. Notice the remarkable improvement over figures 6 a) and b) on the third night. The “hump” has virtually disappeared.

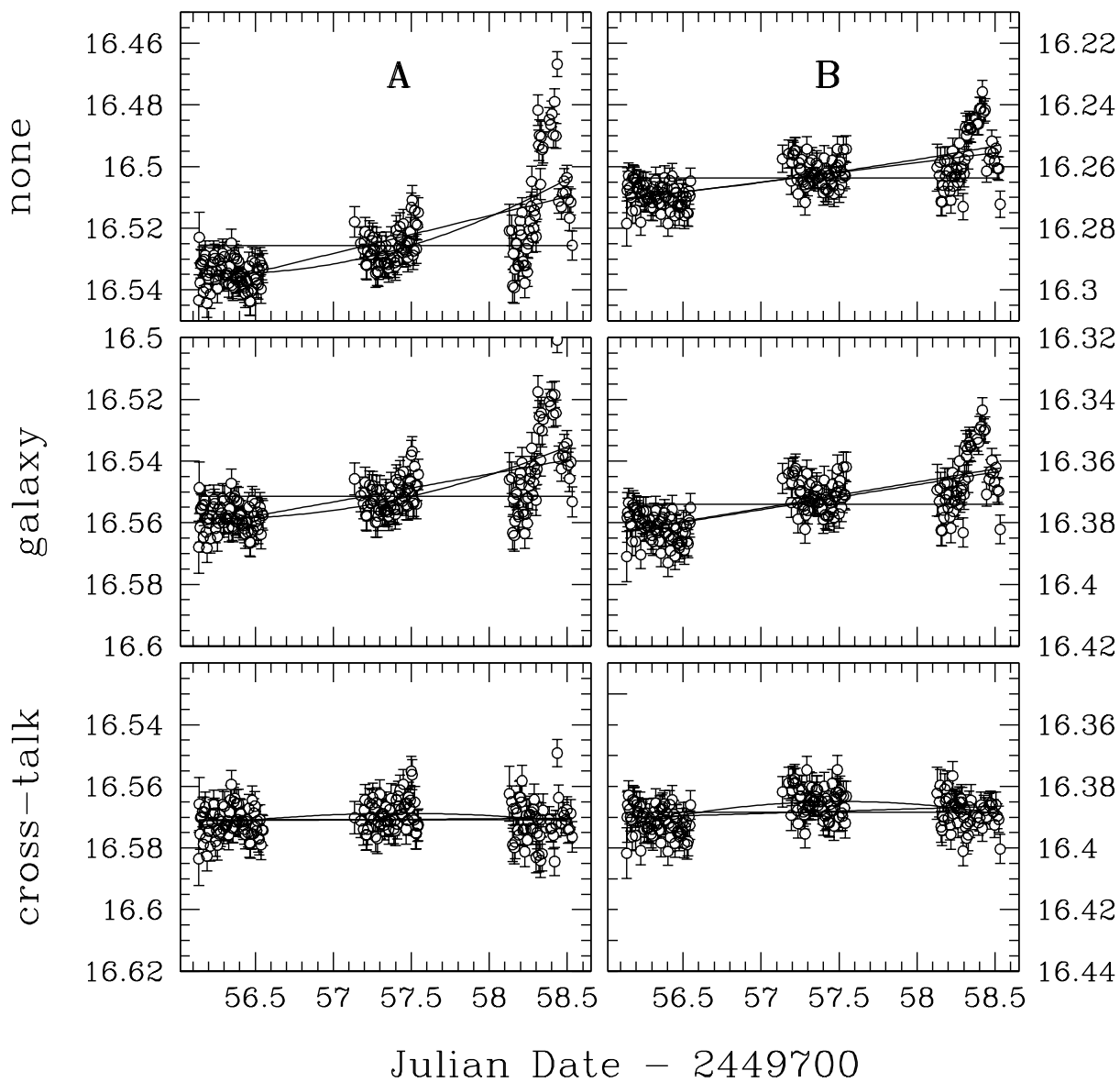


Fig. 7.— The light-curves of images A (left) and B (right), before any correction (top row), after subtraction of the galaxy G1 (middle row) and correction for “cross talk” (bottom row). Overplot are best fits for the mean, a straight line, and for a parabola.